ADVANCES IN ATMOSPHERIC SCIENCES, VOL. 23, NO. 5, 2006, 711–725

Indo-Japanese Lidar Observations of the Tropical Middle Atmosphere During 1998 and 1999

Y. BHAVANI KUMAR*[1], C. NAGESWARA RAJU[2], and M. KRISHNAIAH[2]

[1] *National MST Radar Facility, P. B. No:* 123, *Tirupati*–517 502, *A. P. India*

[2] *Department of Physics, S.V. University, Tirupati*–517 502, *A. P. India*

(Received 12 July 2005; revised 14 February 2006)

ABSTRACT

A state-of-the art Rayleigh and Mie backscattering lidar was set up at Gadanki (13.5°N, 79.2°E) in the Tropics in India. Using this system, regular observations of upper tropospheric clouds, aerosols at stratospheric heights and atmospheric temperatures in the range from 30 to 80 km were made. In this paper, the data collected during the period of 1998–99 were selected for systematic investigation and presentation. The Mie scattering lidar system is capable of measuring the degree of depolarization in the laser backscattering. Several tropical cirrus cloud structures have been identified with low to moderate ice content. Occasionally, thin sub-visible cirrus clouds in the vicinity of the tropical tropopause have also been detected. The aerosol measurements in the upper troposphere and lower stratosphere show low aerosol content with a vertical distribution up to 35 km altitude. Rayleigh-scattering lidar observations reveal that at the tropical site, temperature inversion occurs at mesospheric heights. Atmospheric waves have induced perturbations in the temperatures for several times at the upper stratospheric heights. A significant warming in the lower mesosphere associated with a consistent cooling in the upper stratospheric heights is observed particularly in the winter season during the events of sudden stratospheric warming (SSW).

Key words: backscatter lidar, tropical atmosphere, cirrus, stratospheric aerosol, gravity waves, middle atmospheric temperatures, upper stratospheric cooling

doi: 10.1007/s00376-006-0711-0

1. Introduction

Over the past two decades, a great deal of development has been made in the field of remote sensing of the Earth's atmosphere. Several measurement techniques have been extensively used to better understand the global atmosphere. Among them, the lidar technique has been found to be a potential remote sensing method for probing the atmosphere. Earlier studies have been made on high-altitude cirrus clouds (Beyerle et al., 2001a; Bhavani Kumar et al., 2001), polar stratospheric clouds (Beyerle et al., 2001b; Santacesaria et al. 2001), stratospheric aerosols (Barnes and Hofmann 2001), tropospheric aerosols (Barnaba and Gobbi 2001) and middle atmospheric temperatures (Duck et al., 2000a, 2000b, 2001; Bhavani Kumar et al., 2000; Siva Kumar et al., 2001) by using the backscattering lidar technique.

A typical backscatter lidar transmitter employs pulsed laser light for a vertical sounding of the atmosphere to make range-resolved remote measurements. The laser radiation interacts with various constituents of the atmosphere in a number of different ways. Different types of optical processes in the atmosphere are related to different types of light scatterings (Measures, 1984). In the case of backscattering lidar, laser radiation gets scattered elastically (i.e., with no change in wavelength) from molecules (Rayleigh scattering) and particles (Mie scattering) in the atmosphere and also scattered inelastically from molecules (Raman scattering) with a change in the wavelength. The receiver part of the lidar collects the backscattered laser radiation, converts the light into an electrical signal, and processes it to provide a range-resolved spatial distribution of the atmospheric composition. Depending on the design of the lidar, a variety of atmospheric

*E-mail: ypbk@narl.gov.in

parameters may be measured, including aerosol and cloud properties, temperatures and species concentration.

One of the potential applications of lidar is in the studies of characterization of clouds. Usually strong backscattering arises from clouds due to the relatively large scattering cross-sections of cloud particles and the huge number density of scatterers. Lidar has the capability to delineate the position and spatial structure of clouds in the atmosphere. Because of its high spatial resolution, it can be used to locate the cloud base and its top with a good precision that is not possible with any other remote sensing technique. This feature of lidar has attracted more researchers recently in investigations of clouds at various height regions, as clouds play a critical role in the radiation budget of the Earth's atmosphere (Liou, 1986). The recent reports on backscatter lidar employed in studies of upper tropospheric clouds (Nee et al., 1998; Winker and Trepte, 1998; Platt et al., 1998; Boehm and Verlinde, 2000; Bhavani Kumar et al., 2001; Roumeau et al., 2000) indicate the potential application of the instrument in cloud research.

Another active area where the backscatter lidar has prospective applications in atmospheric research is in the spatial and temporal evolution of dust particles or aerosols. Atmospheric aerosols play a substantial role in the radiative forcing of the Earth's climate, as they influence the radiation balance through the processes of scattering and absorption (Ackerman and Chung, 1992). Extensive studies on atmospheric aerosol distribution in the troposphere and stratosphere have been reported using the backscatter lidar technique (Takamura et al., 1994; Merenco et al., 1997; Barnes and Hofmann, 1997; Nagai et al., 1997; Guzzi et al., 1999) and show the utility of the instrument in atmospheric aerosol research. Recently aerosol clouds in the stratosphere have attracted much attention in the scientific community, because these clouds (McGee et al., 1993; Hofmann et al., 1989) have a definitive impact on climate in destroying the stratospheric ozone. Several studies on the temporal decay of stratospheric dust clouds and polar stratospheric clouds by using backscatter lidar have also been reported (Nagai et al., 1997; Jäeger, 1992; Jäeger et al., 1995).

Significant geophysical information on the structure and dynamics of the atmosphere has been obtained using a variety of instrumental and observational techniques. Basically the atmospheric structure and dynamics are governed by an intense wave activity on a wide range of scales. In the past, high-powered MST (Mesosphere-Stratosphere-Troposphere) radars have yielded high-resolution measurements on wave induced wind fluctuations in the troposphere and lower stratosphere (Balsley and Carter, 1982). But the altitude region between 30 and 60 km is beyond the capability of these radars due to very weak backscatter arising from this range. Several studies on the stratosphere and mesosphere thermal structure have been studied using both space-borne and ground-based instruments (Barnett and Corney, 1985a, 1985b; Mohan Kumar, 1994; Chakravarty et al., 1992). However height profiles of temperatures in the middle atmosphere are observable only from the Rayleigh–scattering lidar technique, except for rocket sounding, which is expensive and not suitable for continuous measurements. Rayleigh backscattering of a laser beam, a basic technique employed by the Rayleigh–scatter lidar, allows us to measure density and temperature profiles (Chanin and Hauchecorne, 1984; Jenkins et al. 1987) in the height range of 30 to 80 km of the atmosphere on a continuous basis with an accuracy better than any other available observational technique. Over the past two decades, it has been observed that the application of Rayleigh-scatter lidar to middle atmosphere investigations is the only reliable technique capable of measuring middle atmospheric temperatures on a long-term basis (Hauchecorne et al., 1991; Leblanc et al., 1998).

The equatorial atmosphere is the region where a considerable Troposphere-Stratosphere Exchange (STE) takes place during the active convection periods. Since convection is a common feature of this region, substantial geophysical information on the structure and wave-induced dynamics in this region of the atmosphere is vital for studying the impact on climate. Presently, this area is blank as far as lidar observations are concerned. Recently an operational lidar system has been installed at the National MST Radar Facility (NMRF) in Gadanki (13.8°N, 79.2°E), which is a tropical site in India, under a Joint scientific collaboration programme between NMRF, India, and the Communications Research Laboratory (CRL), Japan, for regular investigations of the tropical atmosphere. The system became operational in March 1998. The purpose of this paper is to present the composite observations obtained using this system during a one-year period spanning 1998–99. As we are presenting the composite results for the first time, we include technical details of the system also for the benefit of the users of the system in the future.

2. System description

The lidar system was installed at NMRF by CRL in mid March 1998. The complete system configuration is shown in Fig. 1 and the detailed specifications are given in Table 1. The lidar transmitter subsystem is an Nd:YAG pulsed laser with a second harmonic generator (Powerlite 8020: Continuum). The output

Table 1. Major Specifications of the Indo-Japanese Lidar.

Transmitter		
Laser Source		Nd: YAG, Continuum, USA
Operating Wavelength		532 nm
Average energy per pulse		550 mJ
Pulse width		7 ns (Typical)
Pulse repetition rate		20 Hz
Beam Divergence		<0.1 mrad
(Including beam expander)		
Receiver	Rayleigh-scatter Lidar	Mie-scatter Lidar
Telescope type	Newtonian	Schmidt-Cassegrain
Diameter	750 mm	350 mm
Field of View	1 mrad	1 mrad
I F Filter (BW)	1.07 nm	1.13 nm
Signal and Data Processing		
4 channel PC-based photon counting system operating under EG&G MCS real-time software		
Bin width (Range Resolution)	2 μs (300 m)	
Integration time	250 s (corresponding to 5000 laser shots)	

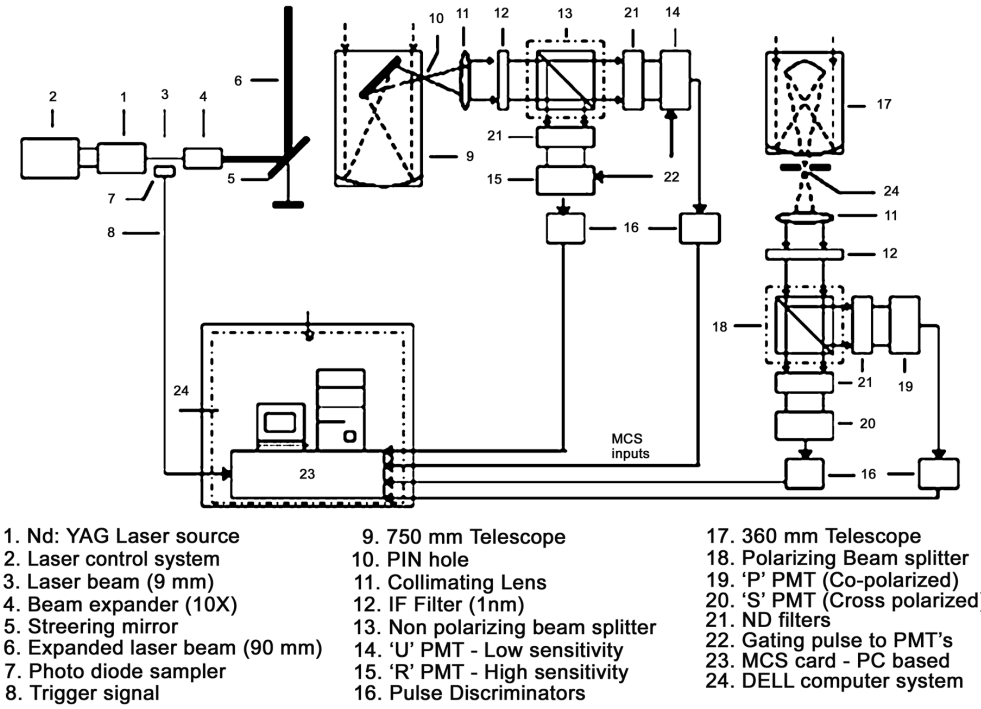

Fig. 1. Block diagram of Indo-Japanese lidar system.

energy of the frequency-doubled 532-nm laser pulse is 550 mJ in repetition of 20 Hz. The laser pulses are transmitted to the zenith by a steering mirror after the beam divergence is reduced to lower than 0.1 mrad through a beam expander (×10).

The NMRF-CRL lidar employs two independent receivers for collecting the laser-backscattered returns from the atmosphere. One of these is a Rayleigh-scatter receiver that collects molecular backscatter in the height range of 30–80 km, whereas the other one is a Rayleigh-Mie scatter receiver that operates in the height range of 4–40 km to receive the backscatter from

air molecules and aerosol/cloud particles.

The Rayleigh-scatter receiver employs a Newtonian configured telescope as a front end. Its primary mirror diameter is 750 mm with an f-ratio of 3:1. The Field of View (FOV) is limited to 1.0 mrad by an aperture put at the focus point of the telescope. On the one hand, the large FOV includes much of the background sky noise, but, on the other hand, it permits a large tolerance for axis adjustment. The light through this aperture is collimated and passes through a narrow band filter with a center wavelength of 532 nm with an full width at half maximum (FWHM) bandwidth of 1.07 nm. To extend the dynamic range of the detectors, the NMRF-CRL system uses a differential non-polarising beam splitter (9:1) to direct the incoming radiation to two similar photomultiplier tubes of dissimilar gains. The 10% channel (low sensitivity—designated as the U Channel) is used to collect the signals from the lower altitudes (25 to 50 Km), whereas the 90% channel (high sensitivity—designated as the R Channel) collects returns from higher altitudes (35 to 90 km). The detector is a low noise PMT (photomultiplier tube, Hamamatsu R3234-01). As the telescope is situated about 2 m away from the steering mirror, the laser returns from altitudes below 5 km are rejected by the aperture. Moreover, we employ an electrical gating up to the altitude of 12 km to protect the PMTs against intense light signals. Because of the adoption of a low signal-induced noise type PMT and a biaxial configuration, there is no need for any mechanical chopper. This makes the system simple and allows for easy operation.

The Mie-scatter receiver is comprised of a portable Schmidt-Cassegrain catadioptic telescope with a clear aperture of 350 mm. The lidar system is configured to operate in a vertical mode with height coverage from 4 to 40 km. The receiver telescope FOV is 1 mrad and the physical separation between the receiver axis and that of the transmitter is 1 m. Though the full overlap of the transmitted and received beams occurs at an altitude of about 4 km above the lidar site, the useful data range is only from 10 to 40 km due to the loading of the detector from the presence of the large number of aerosols at lower tropospheric heights. The laser-backscattered light from particles and molecules is collimated by a lens and passed through an interference filter with a 1.13 nm FWHM bandwidth. A polarized beam splitter—providing polarization diversity—divides the collected laser backscatter returns into co- (P-Channel) and cross-polarized (S-Channel) signal components. Two identical low noise photomultiplier tubes (HAMAMATSU R3234-01) are used as detectors for the linear and orthogonal polarized backscattered signals.

We use photon counting for signal detection. The pulse signals from the PMTs are amplified and discriminated using pulse discriminators. A four-channel (for the P, S, R and U channels) PC based multichannel scaler (MCS plus-EG and G Ortec photon counter) records the counting rate of pulses from the PMT as a function of time. The dwell time of each time bin is set to 2 μs, which corresponds to a range resolution of 300 m, and the maximum number of time bins is set to 1024. The averaged photo-count data in the latter half of the time bins is used for estimation of the background noise.

We normally accumulate the data for a 250-s duration for each measurement, corresponding to 5000 laser firings, which constitute the basic lidar signal. Figures 2a and b are, respectively, sample basic signal profiles from the P and U channels of the Mie and Rayleigh-scatter receivers covering a height range of 150 km. Usually the background noise is estimated for each measurement and subsequently subtracted from the signal for correction. Several of such noise-corrected signal profiles are integrated further for lidar signal analysis. A detailed description of the system and data processing is given elsewhere by Bhavani Kumar et al. (1999).

3. Results and discussion

The Indo-Japanese Lidar (IJL) has been measuring upper-tropospheric clouds and the stratospheric aerosol backscatter at a wavelength of 532 nm with dual polarization since March 1998. The basic lidar signal represents the total backscatter that contains returns from both molecules and particles in the atmosphere. The particulate part of the atmosphere represents either aerosols or clouds composed of ice crystals or hydrometeors. The strength of aerosol or cloud backscatter is usually represented in terms of the backscatter ratio. The noise-corrected lidar signal is subjected to range normalization and inversion (Fernald, 1984) to derive the backscatter ratio profile. Fernald's approach for inverting the lidar signal to derive aerosol backscattering profiles assumes that the aerosol size distribution and composition do not vary with height and that the extinction-to-backscatter ratio of the aerosol, S_a=$\alpha_a(z)/\beta_a(z)$, is a constant over the range. The inversion method basically takes a reference or calibration altitude at which the backscattering coefficient is mainly due to molecules and then performs a downward integration to get the height profiles of $\beta_a(z)$. Here S_a is taken as 40 (Takamura and Sasano, 1987) and the inversion is done downwards from the reference altitude, which is usually taken above 35 km altitude. The backscatter ratio (R) is

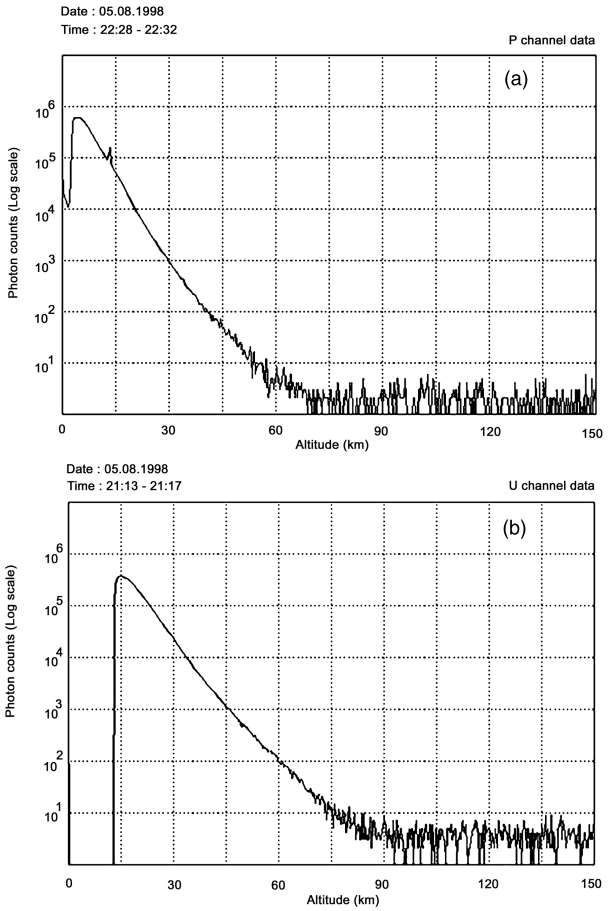

Fig. 2. Typical basic photon count profiles from (a) Mie and (b) Rayleigh-scatter lidar. Each profile is 5000-laser shot integration over 250-s duration.

calculated from the sum of the Mie (particle or aerosol) and Rayleigh scattering coefficients (molecular) divided by the Rayleigh backscatter coefficient, and is given by

$$R(z) = \frac{\beta_{\text{air}}(z) + \beta_{\text{aerosol}}(z)}{\beta_{\text{air}}(z)}$$

where $\beta_{\text{air}}(z)$ and $\beta_{\text{aerosol}}(z)$ represent the volume backscatter cross sections for particles and molecules at altitude z, respectively. Radiosonde pressure and temperature data obtained from the nearest meteorological station, Chennai, approximately 125 km, southeast of the lidar site, are used to derive the air molecular density data. Each lidar data profile is calibrated by performing a linear regression of the measured signal to a theoretical molecular backscatter profile derived using the radiosonde data (Young, 1995). Another lidar-derived quantity, volume depolarization (D), is estimated from the linear and orthogonal aerosol backscatter signals. The signal received from the P channel represents the co-polarized component that arises from molecules and aerosols, which are isotropic scatterers. The signal from the S channel is mainly due to scattering from the anisotropy of the scatterers. The lidar-derived volume depolarization $D(z)$, computed from the backscatter ratios of the co- and cross-polarized signal components, is defined as

$$D(z) = K\frac{S_v(z)}{S_h(z)}$$

where the subscripts v and h refer to perpendicular and parallel polarized signal components, respectively. The calibration component, K, is equal to a volume depolarization of 1.4% when no particles are present, such as in the case of a pure molecular atmosphere (Young, 1980). It may be noted here that higher values of D, greater than the air depolarization (0.014), indicate non-spherical particles, which are presumably ice crystals.

3.1 *Observations of high altitude clouds*

The appearance of deep cumulus clouds during convective periods is a common phenomenon at tropical latitudes. Usually the upper portion of convective cumulus clouds contains ice that extends into the fibrous anvil, which at a later stage takes the form of cirrus. The formation of high altitude clouds such as cirrus in the Tropics plays a particularly important role in the Earth's atmosphere radiation budget. Tropical cirrus develops in a variety of forms, ranging from optically thick anvil cirrus which is closely associated with deep convection (Houze, 1993) to optically thin cirrus layers frequently observed near the tropopause (Boehm et al., 1999). Much of the cirrus in the atmosphere, especially in the Tropics, arises from mesoscale convective activity (Houze, 1993). Moreover, the tropical tropopause being a very cold region with temperatures often reaching as low as 190 K, forms a favorable situation for nucleation and condensation processes, leading to the formation of optical thin cirrus in the vicinity of tropopause (Jenson et al., 1996). The IJL system, equipped with polarization diversity, has detected several different structures of tropical cirrus in the altitudes ranging from 10 to 17 km with derived peak volume depolarization in the range of 0.1 to 0.32. Typical Mie-scatter lidar observations of cirrus systems in the nights of 8–9 May 1998 and 11–12 November 1998 are shown in Fig. 3 for discussion. Figures 3 represent the temporal variation of backscatter ratio (R) and volume depolarization (D) as functions of altitude for two night observations made on 8–9 May and 11–12 November 1998 respectively.

In Fig. 3a, a single cirrus layer in the height range of 14–16 km is detected with a peak R of about 9.2 and a maximum D of 18.6. The observation shows

that cloud appeared initially with strong characteristics of R and D, at 2100 LST 8 May 1998 for a period of about an hour and later it decayed in its strength and became too week to detect. After two hours, that is at 0012 LST 9 May, the cloud started building up in strength (more scattering) and formed a significant spatial structure as shown. It is noticed that the R and D within the cloud show a large spatial and temporal variability. Moreover, the presence of larger values of D, which indicates increased anisotropy of the medium, is mainly due to the orientation of nonspherical particles such as ice crystals. Similar temporal and spatial patterns of R and D indicate variations in the density of crystals in the cloud.

Figure 3b shows the observation on 11–12 November 1998 in which two different layers of cirrus structures are observed during their passage over the lidar site. A thin cirrus layer occurred in the altitude range of 16 to 16.5 km, which appeared to be very close to the tropical tropopause, and persisted for about 5 h. A maximum R of 3.7 with a peak volume depolarization ratio of 0.22 is noted within this cirrus layer. Such layers are generally very thin, with very small optical depth. Hetero-molecular nucleation of aerosols at extremely cold temperatures of the equatorial atmosphere could be the probable reason for the formation of such sub-visible type cloud structures as discussed in detail by Jensen et al. (1996). These thin cirrus layers contribute significantly to the radiation budget and thereby to the warming of the atmosphere (Cess et al., 1990; Stephens and Greenwald, 1991). The other cirrus layer is identified in the altitude range of 12 to 14 km, shown in Fig. 3b as a patchy type of cirrus bands. A peak linear depolarization ratio of 0.17 is observed within these cirrus cloud bands. Larger values of R occasionally observed with lower values of depolarization indicate the presence of either supercooled water droplets or plate crystals (Platt et al., 1998) at that altitude. A typical observation of this kind is noticed at 0519 LST 12 November 1998 as shown in Fig. 4. The radiosonde data (shown in Fig. 4) obtained from the nearest meteorological station, Chennai, indicated that the mid-cloud temperatures are in the range of $-60°$C to $-75°$C. These clouds are generally thick and are observed with an extension of their base with time as fragmented cloud structures, as seen in Fig. 3b. It is also observed that clouds occurring at lower heights (higher temperatures) have lower volume depolarization than clouds observed at higher altitudes (lower temperatures). It indicates that tropical cirrus cloud LDR (linear depolarization ratio) is strongly dependent on the ambient temperature conditions (Platt et al., 1998). The polarization lidar investigations at the Gadanki site reveal that low to moderate values of volume depolarization ratios are detected within tropical cirrus clouds. These results are consistent with the earlier investigations (Takahashi and Kuhura, 1993;

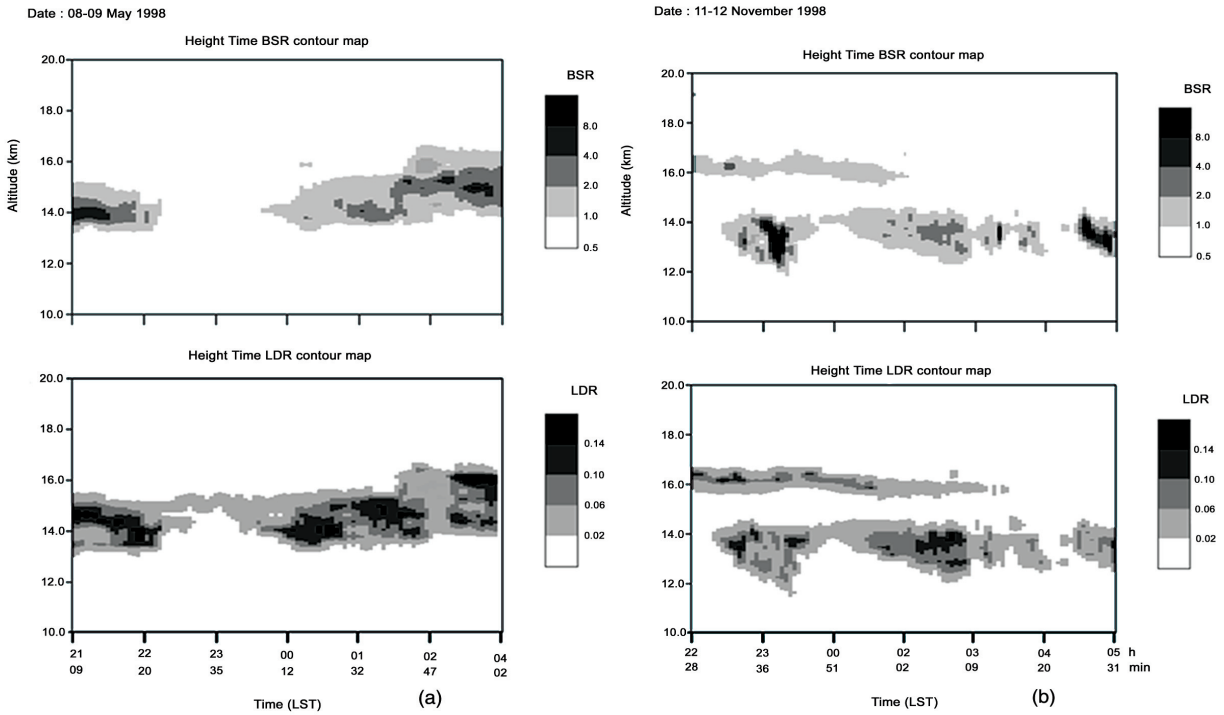

Fig. 3. Temporal variation of cloud Backscatter ratio (R) and Volume Depolarisation (D) as function of altitude for the days (a) 8–9 May 1998 and (b) 11–12 November 1998.

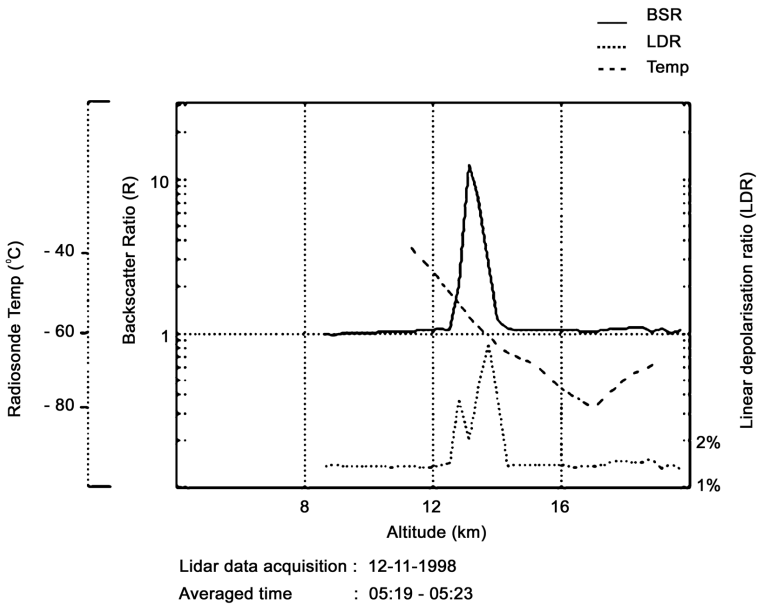

Fig. 4. Height profile showing cloud Backscatter ratio (R) Volume Depolarisation (D) at 0519 LST 12 Nov 1998 as observed by lidar. Radiosonde temperatures also shown in dashed lines to indicate cloud temperature.

Knollenberg et al., 1993; Bhavani Kumar et al., 2001) that reported tropical cirrus observed with low ice water content. Simultaneous lidar and MST radar observation of tropical cirrus (Bhavani Kumar et al., 2001) has shown clearly that the boundaries of cirrus are associated with enhanced vertical shear of horizontal winds and are moreover accompanied by low vertical velocity. The horizontal winds are seen to be enhanced close to the the cloud boundaries. Thus, a circulation is observed at the cloud boundaries indicating entrainment processes at such boundaries.

The polarization Mie-scatter lidar system installed at the tropical site Gadanki has been successfully used to detect the occurrence of high altitude clouds in the range from 10 to17 km during 1998 and 1999. The lidar has identified several tropical cirrus structures with low to moderate scattering and LDR values.

3.2 *Measurement of stratospheric aerosol*

Typical height profiles of the aerosol backscatter ratio integrated over a two-hour period as observed by the Indo-Japanese lidar on the nights of 16 March, 16 October, 28 December 1998 and 19 January 1999 are shown in Fig. 5. Each lidar profile is shown with a corresponding radiosonde temperature profile that is obtained from the nearest meteorological station, Chennai, to identify the local tropopause altitude. The horizontal arrows indicate the altitude of the cold-point tropopause obtained from these temperature measurements. A significant observation from these height profiles is the extended vertical distribution of stratospheric aerosol. There are no noticeable sharp enhancements in aerosol backscatter observed at the stratospheric heights. This confirms that during the time of our observations, the tropical upper troposphere and stratosphere over Gadanki appears free from volcanic aerosols and what we observe now are the background variable aerosol concentrations (Barnes and Hofmann, 1997, 2001; Jäeger and Homburg, 1998). Another significant observation in the backscatter profiles is a noticeable minimum in backscatter ratio (BSR) at the height marked as the local tropopause. A sharp gradient in the temperature accompanied by the tropical tropopause may be the probable reason for such a minimum in the aerosol concentration. The horizontal bars show the standard error dR in the measurements of R for a few sample heights for clarity. Typically, for clear-sky conditions, the BSR standard deviation at low altitudes (10–11 km) is $\sim$0.02 and increases to 0.035 at high altitudes (34–35 km). This rise in the standard deviation is due to the exponential decay in the signal counts with altitude.

The Mie-scatter lidar measurements of stratospheric aerosol made at Gadanki during 1998 and 1999 have been presented in terms of backscatter ratio profiles. The lidar observations over Gadanki confirm that a background aerosol layer existed in the lower strato-

sphere between 18 and 35 km altitude.

3.3 *Measurement of Upper stratospheric and Lower Mesospheric temperatures*

The basic technique used for temperature retrieval from the density profiles is based on the theory described by Hauchecorne and Chanin (1980) and Wilson et al. (1991). At altitudes above 30 km, the Mie-scattering from the aerosol component is negligible and basic scattering arises from the molecular part of the atmosphere. Laser backscatter from atmospheric molecules undergoes Rayleigh scattering and is directly proportional to the molecular number density. The derived relative density profiles are simply corrected for range-squared dependence and normalized at a reference altitude. Absolute temperatures are derived from the density measurements by assuming that the atmosphere is in hydrostatic equilibrium and by integrating the Ideal Gas Law from the greatest altitude downward. The downward integration is triggered from the top using a model pressure value. For this purpose, we have used an atmospheric model, COSPAR International Reference Atmosphere-1986 (CIRA-86), corresponding to respective latitude and monthly values (Fleming et al., 1990). The temperature at altitude z_i in a layer of Δz is given by Jenkins et al. (1987):

$$T(z_i) = \frac{Mg(z_i)\Delta z}{R\ln(1+X)} ,$$

where $g(z_i)$ is the acceleration due to gravity, M is the mean molecular weight, Δz are multipliers, R is the gas constant and X is

$$X = \frac{\rho(z_i)g(z_i)\Delta z}{\sum \rho(z_j)g(z_j)\Delta z + P_m(zn + \Delta z/2)} ,$$

where $\rho(z_i)$ is the atmospheric density and $P_m(zn + \Delta z/2)$ is the reference pressure at the top of the top layer. As seen in the expression of X, the contribution of the reference pressure decreases rapidly with altitude. At heights within about 15 km of the highest altitude the accuracy of the temperature determination is least affected by the choice of initial pressure required to seed the integration (Jenkins et al., 1987). Hence absolute atmospheric temperatures can be deduced from the observed relative densities. Figures 6 are respectively the profiles of temperature and standard error derived from Rayleigh-scatter lidar data integrated over a period of two hours. It is a composite temperature profile constructed using data from the low sensitivity channel (U) for altitudes below 40 km, from the high sensitivity channel (R) above 47 km, and from both channels between 40 and 47 km. A weighting function based on the convex convergence

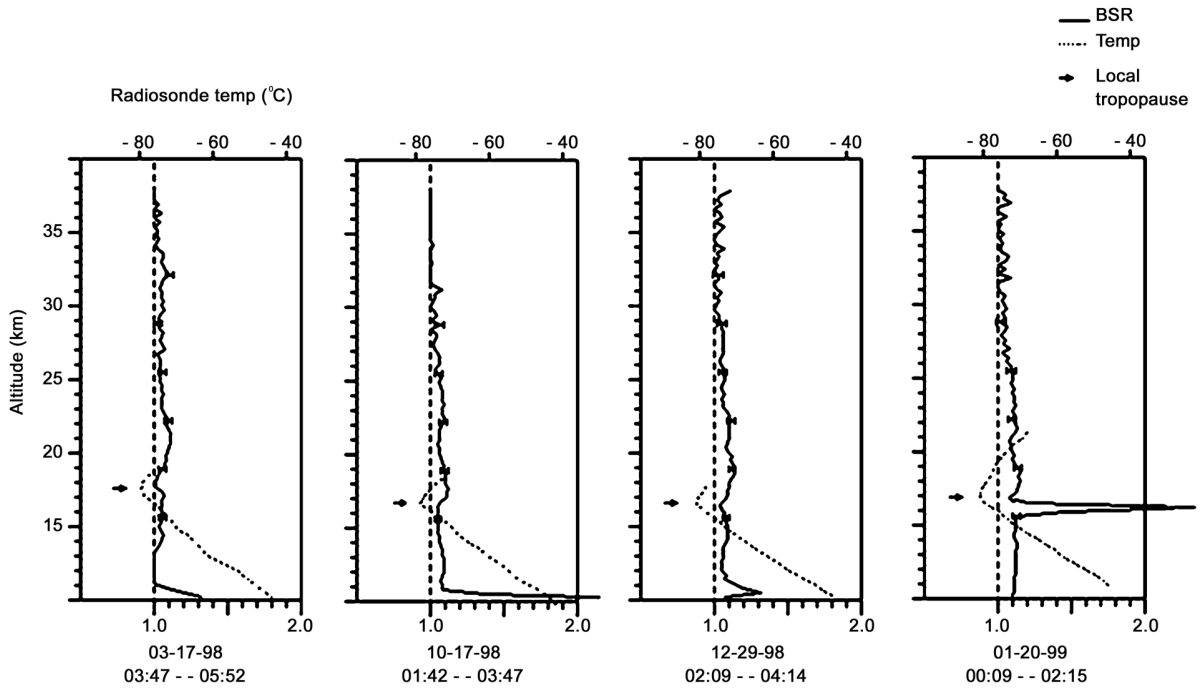

Fig. 5. Height profiles of aerosol backscatter ratio integrated over 2-Hour period as seen by lidar on 16–17 March, 16–17 October, 28–29 December 1998 and 19–20 January 1999.

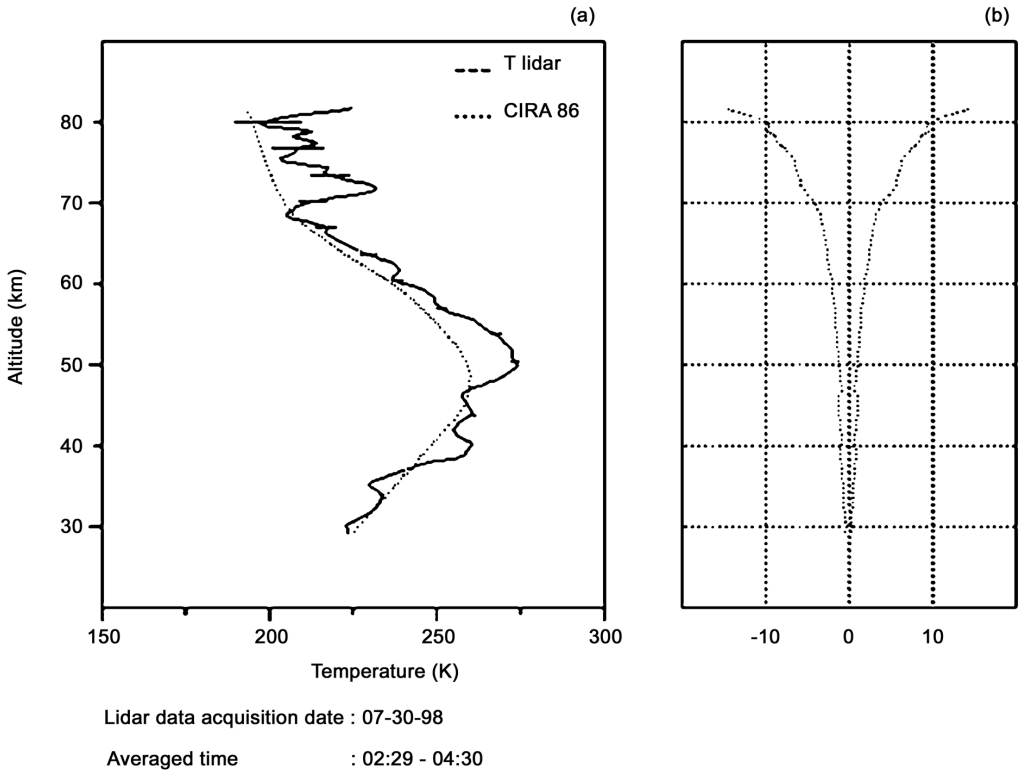

Fig. 6. A composite temperature profile (solid line) derived using Rayleigh-scatter lidar data shown along with model atmosphere data (dotted line) and standard error in temperature.

technique (Bhavani Kumar et al. 2000) is used for a smooth transition between 40 and 47 km. Using the weight factors, the temperature and standard error in temperature for the transition region are expressed as:

$$T_{(40-47)}(z) = \frac{T_{\rm R}(z)\delta T_{\rm U}(z) + T_{\rm U}(z)\delta T_{\rm R}(z)}{\delta T_{\rm R}(z) + \delta T_{\rm U}(z)}$$

and

$$\delta T_{(40-47)}(z) = \frac{T_{\rm R}(z)\delta T_{\rm U}(z) + T_{\rm U}(z)\delta T_{\rm R}(z)}{T_{\rm R}(z) + T_{\rm U}(z)} \ ,$$

where $T_{\rm R}$, $\delta T_{\rm R}$, $T_{\rm U}$ and $\delta T_{\rm U}$ are the derived temperature and standard error in temperature from the R and U channel data respectively. The data used in the present study are taken from the observations made during the period from March 1998 to March 1999. As mentioned previously, we have 80 nights of observations made during this period. It is estimated that the standard errors in hourly mean temperatures are about 0.2 K and 5 K at 30 and 70 km, respectively. The measurement range is normally limited to altitudes above 30 km due to the presence of aerosols and to altitudes below 80 km because of the rapid diminishing of signal strength. Figure 7 shows the sequences of half-hour integrated temperature profiles for the nights of 21–22 October, 21–22 May and 7–8 February 1999 representing the periods of equinox, summer and winter. For October, a localized warming near the stratopause with maximum temperature is found to be around 275 K. For May, there is a clear wave perturbation at lower stratospheric heights with quite a broad stratopause. For February, there is a clear wave-perturbed temperature profile causing lower mesosphere warming followed by upper stratospheric cooling.

The temperature profiles obtained by Rayleigh-scatter lidar frequently exhibit a strong temperature inversion of 20–40 K at mesospheric heights. The mesospheric temperature inversion is an interesting feature, first reported from a rocket experiment (Schmidlin, 1976) and more extensively since then using Rayleigh lidar observations (Hauchecorne et al., 1987; Whiteway et al., 1995). Similar observations were reported from mid-latitudes by Hauchecorne et al. (1987) and Leblanc et al. (1998). This was attributed to the gravity wave breaking at these altitudes Hauchecorne et al. (1987), Meriwether and Mlynczak (1995) and Meriwether and Gardner (2000) independently carried out the analysis on mesospheric temperature inversions and gave an explanation in terms of chemical heating caused by the sudden change in ozo-

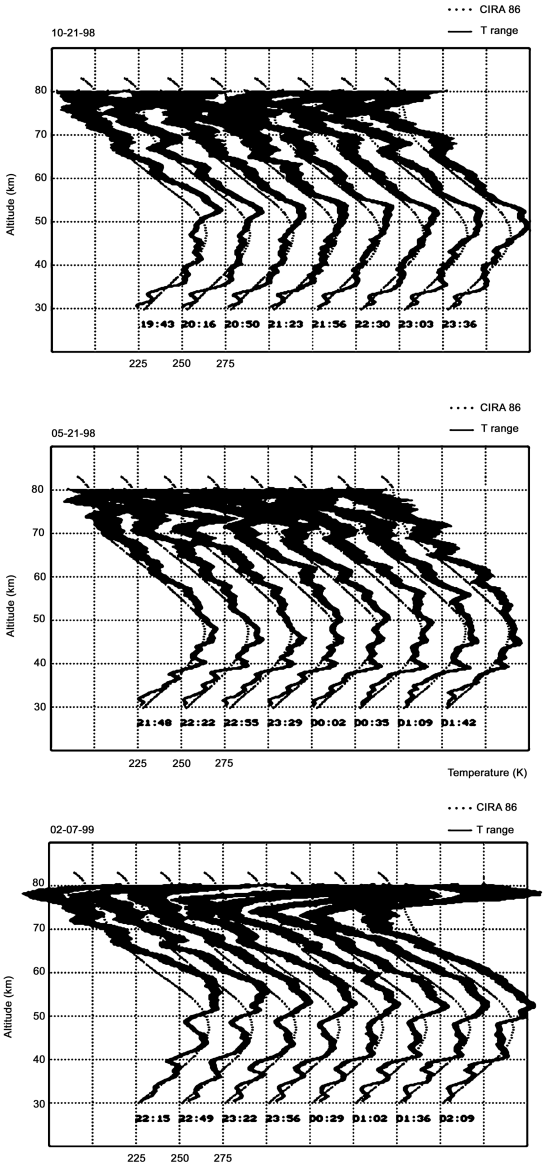

Fig. 7. Sequence of half-hour integrated temperature profiles in the night of 21 October 1998, 21 May 1998 and 7 February 1999 representing summer, equinoctial, and winter periods respectively. Each profile is shifted by 25 K on temperature scale.

ne concentration at these heights. The observations of Hauchecorne et al. (1987) showed that the occurrence of the inversion has a semiannual variation with maxima in summer and winter, and it occurs in the height range of 55–72 km in winter and 70–83 km in summer. The observed inversion was explained by the heating of the turbulent layers generated by the continuous breaking of the upward propagating internal gravity waves. In a subsequent study, however, employing a two-dimensional dynamical model of gravity wave breaking, it was shown that adiabatic heating associated with descending motion is the main mechanism involved in the formation of the mesospheric inversions (Hauchecorne and Maillard, 1990). Recently temperature inversions observed at midlatitudes in the mesosphere by Meriwether and Gardner (2000) and the sodium layer temperatures measured during both the day and night by States et al. (1999) and Chen et al. (2000) have indicated that chemical heating is the major contributor to the mesopause inversions. Temperature inversions at lower altitudes are caused by other mechanisms, and may be related to the diurnal tide (Meriwether and Gardner 2000). In our observations, this inversion always persists above 70 km; sometimes two minima were observed at 4–5 km apart. The midlatitude observations of inversion were reported below 70 km. The observed inversion is always associated with a reduction in the density (Hauchecorne et al., 1987). We observed strong inversions on the order of 20–40 K during equinoctial periods (Bhavani Kumar et al., 2000; Siva Kumar et al., 2001), than compared to summer or winter, which is in contrast with the observations made at midlatitudes (Hauchecorne et al., 1987). The observed temperature inversions at mesospheric heights were found with a minimum persistence of 30 min to more than 7 h indicating that the phenomenon is highly dynamic. In our observations, the temperature variations with a deep minimum around 75 km show a wave-type perturbation whose characteristics seem to conform to that of a gravity wave.

Atmospheric internal gravity waves play an important role in the dynamics of the middle atmosphere and have been observed in the profiles of neutral atmospheric temperatures (Chanin and Hauchecorne 1981; Shibata et al., 1986; Wilson et al., 1991). Previous investigations on gravity wave observations revealed that there is strong interaction between gravity waves, the wind background, and the large-scale thermal structure (Whiteway et al., 1997; Duck et al., 1998, 2000a, b). The Indo-Japanese lidar observation of gravity wave activity in neutral temperatures is shown in Fig. 8a. Sequences of successive basic temperature profiles are plotted over a period of 6 h to indicate the wave-like structures in the temperature profiles of the night of 8–9 May 1998. Significant wave perturbations observed in the temperature profiles of 8–9 May 1998, were considered for the sample wave analysis. The perturbation, $T'(z_i)$ is given by $[T(z_i) - T_0(z_i)]$, where $T(z_i)$ is the basic temperature profile for a 250-s integration and $T_0(z_i)$ is the integrated temperature profile over the whole night. A temporal variation of $T'(z_i)$ (perturbation) plotted as a function of altitude is shown in Fig. 8b. It is clear from this figure that

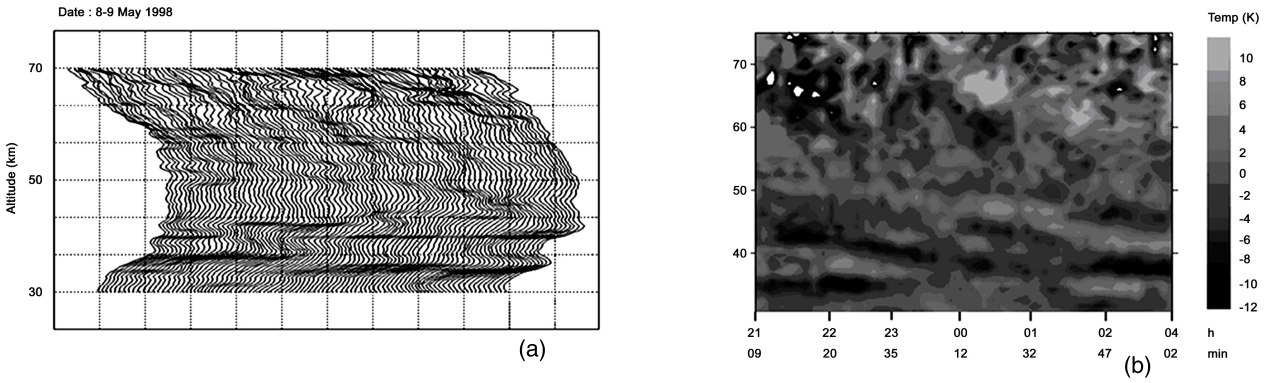

Fig. 8. (a) GW signatures in the Rayleigh-scatter lidar temperatures profiles observed in the night of 8–9 May 1998. Sequences of basic temperature profiles of time duration each 250 s are plotted. (b) A contour map shows the temporal variation of temperature perturbation plotted as a function of altitude.

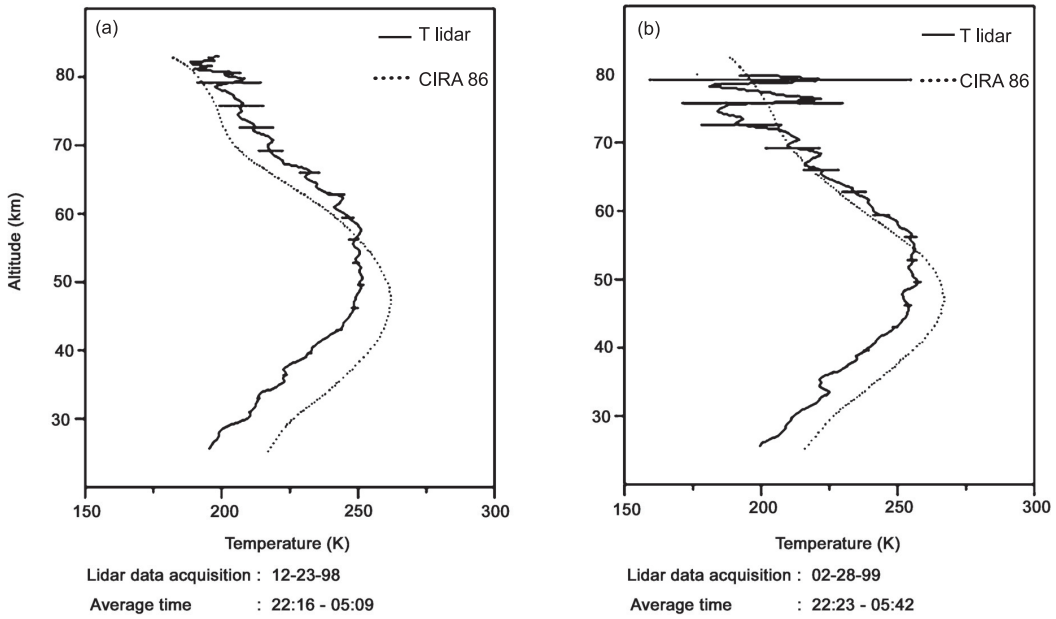

Fig. 9. A sample height profiles of temperature showing the depth of cooling at upper stratospheric heights observed by lidar on (a) 23 December 1998 and (b) 28 February 1999.

some temperature structures (e.g., 43–35 km, 52–46 km) seem to propagate downward, indicating the existence of upward-moving gravity waves. The wave perturbations show a gravity wave type with a vertical wavelength of about 10 km with a downward phase progression seen in the lower height range of 30–50 km. These data show that the instrument has sufficient capability to study atmospheric fluctuations like gravity waves and tides.

Another unusual feature was observed in the profiles of temperature during the winter period of 1998 and 1999. A substantial cooling in the height profiles of temperatures was noticed on 23 December 1998 and 28 February 1999 as shown in Fig. 9. This is about 15 to 20 K lower than the corresponding temperature of the COSPAR International Reference Atmosphere-1986 (CIRA-1986), which represents a monthly zonal mean for December and February at 15°N. We have confirmed that during this period, a strong midwinter warming occurred in the Northern Hemisphere (NH) stratosphere based on zonal mean temperatures for 1998 and 1999 from NOAA(National Oceanic and Atmospheric Administration)-AMSU (Advanced Microwave Sounding Unit) satellite data (http://www.cpc.noaa.gov). Figure 10 shows the AMSU and CPC (climate prediction center) zonal mean 90°–65°N temperatures for 1998 and 1999 at the 1.0 hPa stratospheric level (about 50 km). The zonal mean temperatures were especially high during the stratospheric warming episodes in December 1998 and February 1999. In the Northern Hemisphere (65° to 90°N), stratospheric mid-winter

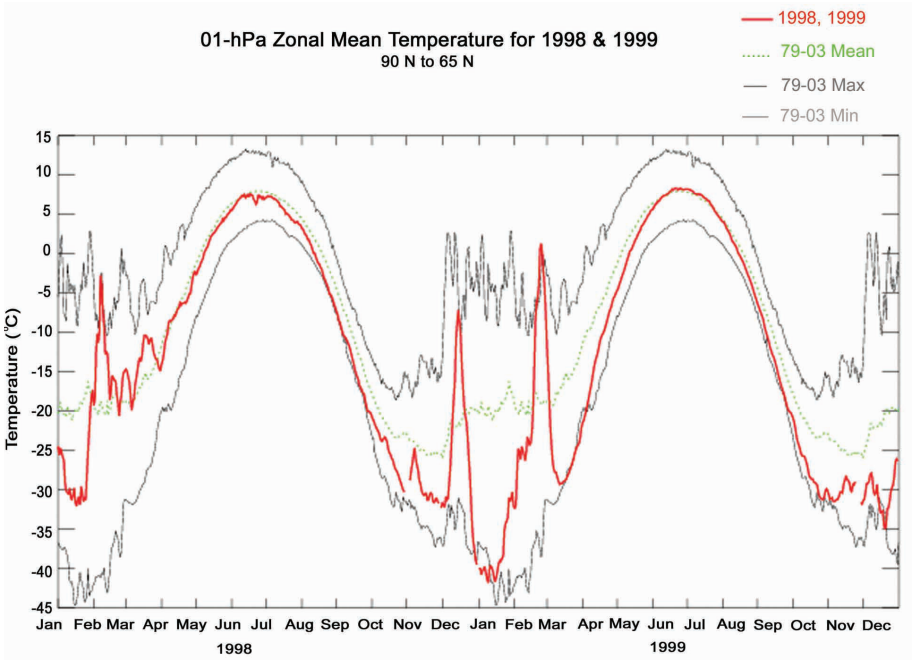

Fig. 10. AMSU zonal mean 65–90N temperatures for 1998 and 1999 at 1 hPa upper stratospheric level. Temperatures were especially high during the stratospheric warming episodes in December 1998 and February 1999.

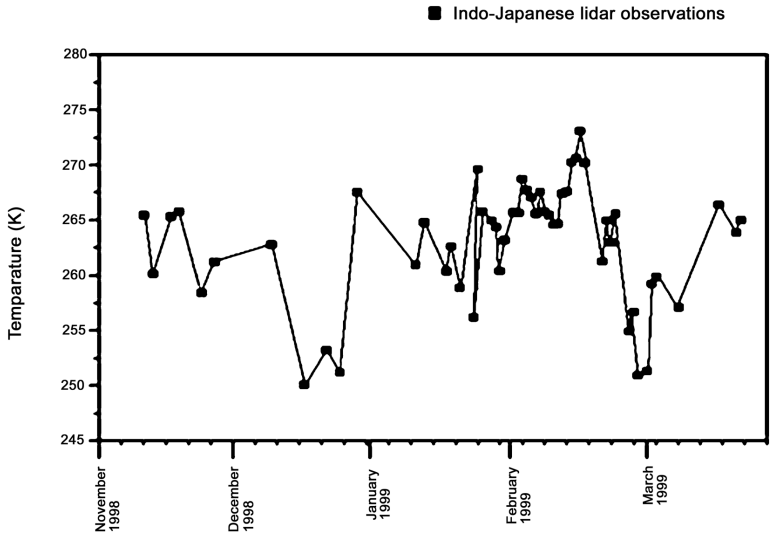

Fig. 11. Indo-Japanese lidar observation of mean temperatures for November 1998 to March 1999 at 50 km altitude. Note that colder temperatures were recorded during stratospheric warming episodes in December 1998 and February 1999.

warmings have been observed between December and March. The nearly continuous measurements of temperature at 50 km altitude obtained from the Indo-Japanese lidar during the period November 1998 to March 1999 are shown in Fig. 11. It is evident from the figure that noticeably lower temperatures were recorded at 50 km altitude during the December 1998 and February 1999 period indicating the association of this event with a warming at polar latitudes. It is now generally accepted that sudden stratospheric

warmings (SSW) are initiated by the propagation of planetary wave disturbances from the troposphere into the stratosphere and mesosphere and their interaction with the mean stratospheric flow (Matsuno, 1971). It is also reported (Hauchecorne and Chanin, 1982) from midlatitude observations that a long wave perturbation such as planetary wave could influence the temperatures of the middle atmosphere.

The temperature measurements derived from Rayleigh-scattering in the range of 30–80 km have been obtained by using the lidar system located at the tropical site Gadanki during 1998 and 1999. The height profiles of temperature were found with wave activities in the upper stratosphere. Significant lower temperatures in the upper stratosphere have been observed over this tropical site during the polar winter warming episodes such as SSW.

4. Summary

By using a Rayleigh- and Mie-backscattering lidar, we have observed high altitude clouds, stratospheric aerosols, and temperatures in the height range of 30–80 km. The polarization Mie-scattering lidar has been used for the detection of tropical cirrus clouds in the altitude range of 10–17 km. These clouds are observed with low to moderate LDR. Usually, the thick cirrus clouds have large scattering ratios observed with enhanced optical depths. Thin cirrus clouds are occasionally detected near the tropical tropopause. The measurement of stratospheric aerosols by the lidar system confirms that during the times of present observation, the tropical upper troposphere and lower stratosphere over the Gadanki site appears free from volcanic aerosols and what we observe now are the background variable aerosols. Rayleigh-scatter lidar observations of temperatures in the upper stratosphere and the lower mesosphere were found to show prominent wave activity. Interesting features such as temperature inversions at mesospheric heights and noticeable cooling in stratospheric temperatures during the stratwarm period were observed over the tropical site Gadanki.

Acknowledgments. The National MST Radar Facility (NMRF) located at Gadanki in India is operated by the Department of Space, Government of India. The authors would like to acknowledge, with thanks, the numerous contributions by their colleagues at the NMRF, India, and the Communications Research Laboratory (CRL), Japan, in successfully operating the lidar facility under an Indo-Japanese collaboration program.

REFERENCES

Ackerman, F., and H. Chung, 1992: Radiative effects of airborne dust and regional energy budget at the top of the atmosphere. *J. Appl. Meteor.*, **31**, 223–233.

Balsley, B. B., and D. A. Carter, 1982: The spectrum of atmospheric velocity fluctuations at 8 km and 86 km. *Geophys. Res. Lett.*, **9**, 465–468.

Barnett, J. J., and M. Corney, 1985a: Middle atmosphere reference model derived from satellite data. *MAP Handbook*, **16**, K. Labitzke, J. J. Barnett, and B. Edwards, Eds., SCOSTEP, 47–85.

Barnett, J. J., and M. Corney, 1985b: Temperature data from satellites. *MAP Handbook* , **16**, K. Labitzke, J. J. Barnett, and B. Edwards, Eds., SCOSTEP, Urbana, 3–11.

Barnes, J. E., and David J. Hofmann, 1997: Lidar measurements of stratospheric aerosol over Mauna Loa Observatory. *Geophys. Res. Lett.*, **24**, 1923–1926.

Barnes, J. E., and D. J. Hofmann, 2001: Variability in the Stratospheric Background Aerosol over Mauna Loa Observatory. *Geophys. Res. Lett.*, 2859–2863.

Barnaba, F., and G. P. Gobbi, 2001: Lidar estimation of tropospheric aerosol extinction, surface area and volume: Maritime and desert-dust cases. *J. Geophys. Res.*, **106 (D3)**, 3005–3018.

Beyerle, G., and Coauthors, 2001a: A lidar and backscatter sonde aerosol measurement campaign at Table Mountain during February–March 1997: Observations of cirrus clouds, *J. Atmos. Sci.*, ***58***, 1275–1287.

Beyerle, G., H. Deckelmann, R. Neuber, J. M. Rosen, E. Reimer, and M. R. Schoeberl, 2001b: Occurrence of solid particles in the winter polar stratosphere above the nitric acid trihydrate co-existence temperature inferred from ground-based polarization lidar observations at Ny-Ålesund, Spitsbergen. *J. Geophys. Res.*, **106**, 2979–2992.

Bhavani Kumar, Y., and Coauthors, 1999: Indo-Japanese lidar system : PartI—System description and Data Processing, *Proceedings of Radar Symposium, India (IRSI),* 560–570.

Bhavani Kumar, Y., V. Siva Kumar , P. B. Rao, M. Krishnaiah, K. Mizutani, T. Aoki, M. Yasui, and T. Itabe, 2000: Middle atmospheric temperature measurements using ground based instrument at a low latitude. *Ind. J. Rad. and Space Phys.*, **29**, 249–257.

Bhavani Kumar, Y., V. Siva Kumar, A. R. Jain, and P. B Rao, 2001: MST radar and polarization lidar observations of tropical cirrus. *Ann. Geophys*, **19**, 873–883.

Boehm, M. T., and J. Verlinde., 2000: Stratospheric Influence on upper tropospheric tropical cirrus. *Geophys. Res. Lett.*, **27**, 3209–3212.

Boehm, M. T., J. Verlinde, and T. P. Ackerman, 1999: On the maintenance of high tropical cirrus. *J. Geophys. Res.*, **104**, 24 423–24 433.

Cess, R. D., and Coauthors, 1990: Intercomparison and interpretation of climate feedback processes in 19 atmospheric general circulation models. *J. Geophys. Res.*, **95**, 16 601–16 615.

Chakravarty, S. C., Jayati Datta, and C. P. Revankar, 1992: Climatology of long-period oscillations in the equatorial middle atmosphere over Thumba, India. *Current Sci.*, **63**, 33–42.

Chanin, M. L., and A. Hauchecorne, 1981: Lidar observation of gravity and tidal waves in the stratosphere and mesosphere. *J. Geophys. Res.*, **86**, 9715–9721.

Chanin, M. L., and A. Hauchecorne, 1984: Lidar studies of temperature and density using Rayleigh scattering. *MAP Handbook*, **13**,87–98.

Chen, S., Z. Hu, M. A. White, H. Chen, D. A. Krueger, and C. Y. She, 2000: Lidar observations of seasonal variation of diurnal mean temperature in the mesopause region over Fort Collins, Colorado (41°N, 105°W). *J. Geophys. Res.*, **105**, 12371–12380.

Collis, R. T. H., 1966: Lidar: A new atmospheric probe. *Quart. J. Roy. Meteorol. Soc.* **92**, 220.

Duck, T. J., J. A. Whiteway, and A. I. Carswell, 1998: Lidar observations of gravity wave activity and Arctic stratospheric vortex core warming. *Geophys. Res. Lett.*, **25**, 2813–2816.

Duck, T. J., J. A. Whiteway, and A. I. Carswell, 2000a: Sudden stratospheric and stratopause warmings: Observations of temperatures in the middle atmosphere above Eureka, in Atmospheric Science Across the Stratopause. *AGU Geophysical Monograph Series*, **123**, 207–212.

Duck, T. J., J. A. Whiteway, and A. I. Carswell, 2000b: A detailed record of High Arctic middle atmospheric temperatures. *J. Geophys. Res.*, **105**, 22909–22918.

Duck, T. J., D. P. Sipler, J. E. Salah, and J. W. Meriwether, 2001: Rayleigh lidar observations of a mesospheric inversion layer during night and day. *Geophys. Res. Lett.*, **28**, 3597–3600.

Fernald, F. G., 1984: Analysis of atmospheric lidar observations: Some comments. *Appl. Opt.,* **23**, 652–653.

Fleming, E. L., S. Chandra, J. J. Barnett, and M. Corney, 1990: Zonal mean temperature, pressure, zonal wind and geo-potential height as functions of latitude. *Adv. Space Res.*, **10**, 1211–1259.

Guzzi, D., M. Morandi, V. Santacesaria, L. Stefanutti, P. Agostini, B. Liley, and J. P. Wolf, 1999: Four years of stratospheric aerosol measurements in the northern and southern hemispheres. *Geophys. Res. Lett.*, **26**, 2199–2002.

Hauchecorne, A., and M. L. Chanin, 1980: Density and temperature profiles obtained by lidar between 35 and 70 km. *Geophys. Res. Lett.*, **7**, 565–568.

Hauchecorne, A., and M. L. Chanin, 1982: A mid-latitude ground based lidar study of stratospheric warmings and planetary waves propagation, *J. Atmos. Terr. Phys.*, **44**, 577–583.

Hauchecorne, A., and A. Maillard, 1990: A 2-D dynamical model of mesospheric inversion in winter. *Geophys. Res. Lett.*, **17**, 2197–2200.

Hauchecorne, A., M. L. Chanin, and R. Wilson, 1987: Mesospheric temperature inversion and gravity wave breaking. *Geophys. Res. Lett.*, **14**, 933–936.

Hauchecorne, A., M. L. Chanin, and P. Keckhut, 1991: Climatology and trends of the middle atmospheric temperature (33-87 km) as seen by Rayleigh lidar over the south of France. *J. Geophys. Res.*, **96**, 15297–15309.

Hofmann, D. J., and Coauthors, 1989: Stratospheric Clouds and Ozone Depletion in the Arctic During January 1989. *Nature*, **340**, 117–121.

Houze, R. A. Jr., 1993: *Cloud Dynamics.* Academic Press, 570 pp.

Jäeger, H., 1992: The Pinatubo eruption cloud observed by lidar at Garmisch-Partenkirchen. *Geophys. Res. Lett.,* **19**,191–194.

Jäeger, H., O. Uchino, T. Nagai, T. Fujimoto, V. Freudenthaler, and F. Homburg, 1995: Ground-based remote sensing of the decay of the Pinatubo eruption cloud at three northern hemsiphere sites. *Geophys. Res. Lett.*, **22**, 607–610.

Jäeger, H., and F. Homburg, 1998: A new aerosol background level in the stratosphere? Lidar observations of the period 1976 to 1997. *19th ILRC*, NASA/CP-1998-207671/PT1, 335–338.

Jenkins, D. B., D. P. Wareing, L. Thomas, and G. Vaughan, 1987: Upper stratospheric and Mesospheric temperature derived from lidar observations at Aberystwyth. *J. Atmos. Terr. Phys.*, **49**, 287–298.

Jensen, E. J., O. B.Toon, H. B. Selkirk, J. D. Spinhirne, and M. R. Schoeberl, 1996: On formation and persistence of subvisible cirrus clouds near the tropical tropopause. *J. Geophys. Res.*, **101**, 21 361–21 375.

Knollenberg, R. G, K. Kelly, and J. C. Wilson, 1993: Measurements of high number densities of ice crystals in the tops of tropical cumulonimbus. *J. Geophys. Res.*, **98**, 8639–8664.

Liou, K. N., 1986: Influence of cirrus clouds on weather and climate processes. *Mon. Wea. Rev.*, **114**, 1167–1199.

Leblanc, T., I. S. McDermid, P. Keckhut, A. Hauchecorne, C. Y. She, and D. A. Krueger, 1998: Temperature climatology of the middle atmosphere from long-term lidar measurements at middle and low latitudes. *J. Geophys. Res.*, **103**, 17191–17204.

Matsuno, T., 1971: A dynamical model of the stratospheric sudden warming. *J. Atmos. Sci.,* **28(8)**, 1479–1494.

McGee, T. J., M. Gross, R. Ferrare, W. S. Heaps, and U. Singh, 1993: Raman DIAL Measurements of Stratospheric Ozone in the Presence of Volcanic Aerosols. *Geophys. Res. Lett.,* **20**, 955–958.

Measures, R. M., 1984: *Laser Remote Sensing, Fundamentals and Applications.* J. Wiley and Sons, New York, 510pp.

Meriwether, S. J. W., and M. G. Mlynczak , 1995: Is chemical heating a major cause of the mesosphere inversion layer? *J. Geophys. Res.*, **100**, 1379–1383.

Meriwether, J. W., and C. S. Gardner, 2000: A review of the mesospheric inversion layer phenomenon. *J. Geophys. Res.,* **105**, 12 405–12 416.

Merenco, F., V. Santacesaria, A. Bais, D. Balis, Papayannis A. di Sarra, and C. S Zerefos, 1997: Optical properties of tropospheric aerosols determined by lidar and spectro-photometric measurements (PAUR campaign). *Applied Optics*, **36**, 6875–6886.

Mohankumar, K., 1994: Temperature variability over the tropical middle atmosphere. *Ann. Geophys.,* **12**, 448–496.

Nagai, T., O. Uchino, T. Itabe, T. Shibata, K. Mizutani, T. Fujimoto and M. Hirota, 1997a: Lidar observations of the PSCs and stratospheric aerosols over Eureka. Canadian Arctic. *Advances in Atmospheric Remote sensing with Lidar*, 505–508.

Nagai, T., O. Uchino, T. Itabe, T. Shibata, K. Mizutani and T. Fujimoto, 1997b: Polar stratospheric clouds observed at Eureka (80N, 86W) in the Canadian Arctic during the 1994/1995 winter. *Geophys. Res. Lett.,* **24**, 2243–2246.

Nee, J. B., C. N. Len, W. N. Chen, and C. I. Lin, 1998: Lidar observations of the cirrus cloud in the tropopause at Chung-Li (25°N, 121°E). *J. Atmos. Sci.*, **55,** 2249–2257.

Platt, C. M. R., S. A. Young, P. J. Manson, G. R. Peterson, S. C. Marsden, T. Austin and J. H. Churnside, 1998: The optical properties of equatorial cirrus from observations in the ARM pilot radiation observation experiment. *J. Atmos. Sci.*, **55**, 1977–1996.

Roumeau, S., P. Bremaud, E. Riviere, S. Baldy, and J. L. Baray, 2000: Tropical cirrus : A possible sink for ozone. *Geophys. Res. Lett.*, **27**, 2233–2236.

Santacesaria, V., A. R. MacKenzie, and L. Stefanutti, 2001: A climatological study of polar stratospheric clouds (1989–1997) from LIDAR measurements over Dumont d'Urville (Antarctica). *Tellus* (B), **53 (3)**, 306–321.

Schmidlin, F. J., 1976: Temperature inversion near 75 km. *Geophys. Res. Lett.*, **3**, 173–176.

Shibata, T., T. Fukuda., and M. Maeda, 1986: Density fluctuations in the middle atmosphere over Fukuoka observed by an XeF Rayleigh lidar. *Geophys. Res. Lett.*, **13**, 1121–1124.

Siva Kumar, V., and Coauthors, 2001: Lidar measurements of mesospheric temperature inversion at a low latitude. *Ann. Geophys.*, **19**, 1039–1044.

States, Robert J., and Chester S. Gardner, 1999: Thermal structure of the mesopause region (80–105 km) at 40N latitude: 2. Diurnal variations. *J. Atmos. Sci.*, **57**, 78–92.

Stephens, G. L., and T. J. Greenwald, 1991: The Earth's radiation budget and its relation to atmospheric hydrology: 2. Observations of cloud effects. *J. Geophys. Res.*, **96**, 15,325–15340.

Takamura, T., and Y. Sasano, 1987: Ratio of aerosol backscatter to extinction coefficients determined from angular scattering measurements for use in atmospheric lidar applications. *Opt. and Quant. Electro.,* **19**, 293–302.

Takahashi, T., and K. Kuhura, 1993: Precipitation Mechanism of cumulonimbus clouds at Pohnpei, Micronesia. *J. Meteor. Soc. Japan*, **71**, 21–31.

Takamura, T., Y. Sasno, and T. Hayakashi, 1994: Tropospheric aerosol optical properties derived from lidar, sun photometer and optical particle counter measurements. *Applied Optics*, **33**, 7132–7140.

Wilson, R., M. L. Chanin, and A. Hauchecorne, 1991: Gravity waves in the middle atmosphere observed by Rayleigh lidar 1. Case studies, *J. Geophys. Res.*, **96**, 5153–5167.

Winker, D. M., C. R. Trepte, 1998: Laminar cirrus observed near the tropical tropopause by LITE. *Geophys. Let.*, **25**, 3351 – 3354.

Whiteway, J. A., A. I. Carswell, and W. E. Word, 1995: Mesospheric temperature inversions with overlaying nearly adiabatic lapse rate : An indication of a well-mixed turbulent layer. *Geophys. Res. Lett.*, **22**, 1201–1204.

Whiteway, J. A., T. J. Duck, D. P. Donovan, J. C. Bird, S.R. Pal, and A. I. Carswell, 1997: Measurements of gravity wave activity within and around the Arctic stratospheric vortex. *Geophys. Res. Lett.* , **24**, 1387–1390.

Young, A. T., 1980: Revised depolarization correction for atmospheric extinction. *Appl. Opt.*, **19**, 3427–3428.

Young, S. A., 1995: Analysis of lidar backscatter profiles in optical thin clouds. *Appl. Opt.*, 34 7019–34 7031.